https://doi.org/10.5194/bg-2021-95
Preprint. Discussion started: 19 April 2021

Biogeosciences Discussions
Open Access

Unveiling spatial and temporal heterogeneity of a tropical forest canopy using high-resolution NIRv, FCVI, and NIRvrad from UAS observations

Trina Merrick[1,4], Stephanie Pau[1], Matteo Detto[2,3], Eben N. Broadbent[4], Stephanie. A. Bohlman[5], Christopher J. Still[6], Angelica M. Almeyda Zambrano[7]

[1] Department of Geography, Florida State University, 113 Collegiate Loop, Tallahassee, Florida 32306, USA
[2] Smithsonian Tropical Research Institute, Apartado 0843–03092, Balboa, Anc´on, Panama
[3] Department of Ecology and Evolutionary Biology, Princeton University, Princeton, New Jersey 08544 USA
[4] Spatial Ecology and Conservation Lab, School of Forest Resources and Conservation, University of Florida, Gainesville, FL, 32608 USA
[5] School of Forest Resources and Conservation, University of Florida, Gainesville, FL, 32608 USA
[6] Department of Forest Ecosystems and Society, Oregon State University, Corvallis, Oregon 97331 USA
[7] Spatial Ecology and Conservation Lab, Center for Latin American Studies, University of Florida, Gainesville, Florida 32608 USA

Correspondence to: Trina Merrick (tmerrick@fsu.edu)

Abstract. Presented here for the first time are emerging vegetation indicators: near-infrared reflectance (NIRv) of vegetation, the fluorescence correction vegetation index (FCVI), and radiance (NIRvrad) of vegetation, for a tropical forest canopy calculated using UAS-based hyperspectral data. Fine-scale tropical forest heterogeneity represented by NIRv, FCVI, and NIRvrad, is investigated using unmanned aerial vehicle data and eddy covariance-based gross primary productivity estimates. By exploiting near-infrared signals, emerging vegetation indicators captured the greatest spatiotemporal variability, followed by the enhanced vegetation index (EVI), then the normalized difference vegetation index (NDVI), which saturates. Wavelet analyses showed the dominant spatial variability of all indicators is driven by tree clusters and larger-than-tree-crown size gaps (not individual tree crowns or leaf clumps), but emerging indices and EVI captured structural information at smaller spatial scales (~50 m) than NDVI (~90 m) and lidar (~70 m). As predicted in previous studies, we confirm that NIRv and FCVI are virtually identical for a dense green canopy despite the differences in how these indices were derived. Furthermore, we show that NIRvrad, which does not require separate irradiance measurements, correlated most strongly with gross primary productivity and photosynthetically active radiation. These emerging indicators, which are related to canopy structure and the radiation regime of vegetation canopies are promising tools to improve understanding of tropical forest canopy structure and function.

1 Introduction

Important spatial and temporal heterogeneity in structurally complex and species-rich tropical forests are not well characterized. Varying microclimate, light conditions, topography, crown structure, and patterns of tree mortality and regeneration, for example, contribute to heterogeneity that underlies gross primary production (GPP) at a coarse scale. Remote sensing (RS) measurements have been employed to uncover vegetation patterns from local to global scales e.g. (Jung et al., 2011; Glenn et al., 2008; Huete et al., 2002; Ryu et al., 2018; Yang et al., 2017; Jiang et al., 2008;

https://doi.org/10.5194/bg-2021-95
Preprint. Discussion started: 19 April 2021

Zhao et al., 2010; Heinsch et al., 2006; Running et al., 2004; Turner et al., 2003). Yet, there is a lack of high spatial and temporal resolution data that can capture fine-grained heterogeneity of tropical forests (Clark et al., 2017; Mitchard, 2018; Saatchi et al., 2011; Lewis et al., 2009). Unpiloted aerial systems (UAS) with hyperspectral imaging sensors present an opportunity to collect tropical forest canopy data at high spatial resolution, which could address unknowns related to the high heterogeneity of tropical forests. Traditional reflectance-based indices (RI) using RS data are known to capture structural changes that are coincident with changes in GPP. RIs from remote sensing platforms have provided optical methods to track GPP via connections using the light use efficiency model (LUE). RIs commonly used in the LUE model of GPP as well as for GPP itself are the normalized difference vegetation index (NDVI) and enhanced vegetation index (EVI) (Springer et al., 2017; Morton et al., 2015; Gamon et al., 2015; Porcar-Castell et al., 2014; Glenn et al., 2008; Gao et al., 2007; Huete et al., 2002; Zarco-Tejada et al., 2013). NDVI and EVI are typically used as proxies on seasonal timescales, or, when used to examine changes on shorter timescales, they have been multiplied by photosynthetically active radiation (PAR) to account for changes in radiation (incoming, absorbed, and scattered) which better align with GPP changes (Springer et al., 2017). However, RIs alone have often not shown enough sensitivity to capture more subtle changes in vegetation, such as those in tropical forests, and questions linger about their ability to track green-up with RIs in tropical regions (Liu et al., 2021; Yang et al., 2018a; Lee et al., 2013; Xu et al., 2015; Morton et al., 2014; Samanta et al., 2010; Sims et al., 2008).

In recent years, solar-induced fluorescence (SIF) has been employed widely to improve our understanding of the productivity, seasonal timing, and structure of vegetated ecosystems because it promises to be a better proxy for GPP than RIs (e.g.(Merrick et al., 2019; Köhler et al., 2017; Sun et al., 2017; Schickling et al., 2016; Guanter et al., 2014; Rossini et al., 2014; Van Wittenberghe et al., 2013; Zarco-Tejada et al., 2012; Guanter et al., 2012; Frankenberg et al., 2011; Joiner et al., 2011; Meroni et al., 2009). SIF is mechanistically linked to photosynthesis of plants and, thereby, has also been shown to be more sensitive to changes in forest canopy function and structure than RIs. However, estimating SIF requires high spectral resolution instruments and a complex retrieval algorithm to extract the SIF signal from reflected radiation reaching the sensor (Merrick et al., 2020; Rong Li, 2016; Julitta, 2015; Cogliati et al., 2015; Liu et al., 2015; Porcar-Castell et al., 2014; Malenovsky et al., 2009; Alonso et al., 2008, 2007; Logan et al., 2007; Moya et al., 2004; Alonso et al., 2003; Zarco-Tejada et al., 2001; Plascyk, 1975). Once extracted, the SIF signal also contains both a physiological component (i.e. the number of fluorescence photons generated as a byproduct of photosynthesis) and structural component (e,g., arrangement of leaves, clumping, and canopy structure, which determine the light capture and SIF photon scattering regime of plants). The aforementioned complexity of measuring SIF and subsequent interpretation limit the number of studies using SIF in comparison to RIs (Hao et al., 2021; Zhang et al., 2020; Magney et al., 2017; Liangyun Liu, 2016; Van Wittenberghe et al., 2015; Baldocchi et al., 2020; Wang et al., 2020; Wu et al., 2020; Badgley et al., 2019). An additional barrier in tropical regions is that SIF data in tropical forests is even more scarce than in other biomes and, likely due to data scarcity and combined complexities of the SIF measurements and heterogeneity of tropical forest canopies, relationships to plant function in tropical forests are even more poorly understood than other biomes (Merrick et al., 2019; Wang et al., 2019; Yang et al., 2018a; Liu et al., 2017; Castro et al., 2020; Köhler et al., 2017).

https://doi.org/10.5194/bg-2021-95
Preprint. Discussion started: 19 April 2021

Biogeosciences Discussions
Open Access

Three emerging vegetation indicators have been shown to track with GPP and SIF more closely than traditional RIs, mainly by effectively capturing the structural component of RS SIF signals reaching the sensor. The structural component of RS SIF signals is represented by

$$fPAR \ x \ f_{esc} \tag{1}$$

where fPAR is the fraction of photosynthetically active radiation (PAR) absorbed by vegetation, and f_{esc} is the escape probability, i.e. the photons that escape the canopy. These indicators are the near-infrared reflectance of vegetation (NIRv) (Badgley et al., 2017), the fluorescence correction vegetation index (FCVI) (Yang et al., 2020) and the near-infrared radiance of vegetation (NIRvrad) (Wu et al., 2020). These vegetation indicators, due to the way they exploit the near-infrared radiation from vegetation, do not saturate in dense canopies and are less sensitive to dead vegetation than traditional RIs, therefore they exceed the capabilities of RIs to yield information about vegetation. Additionally, these emerging indicators require only moderate spectral resolution data, do not require a separate measurement of incoming radiation the way SIF does, and are calculated similarly to traditional RIs, making them accessible in a broad range of studies. Therefore, NIRv, FCVI, and NIRvrad could be employed to separate physiological and structural components of a SIF signal or used to independently as valuable indicators of canopy structure, fPAR, APAR, or SIF scattering (Badgley et al., 2019; Badgley et al., 2017; Dechant et al., 2020).

NIRv is the product of NDVI and the near-infrared reflectance (NIR) and was shown to be empirically related to fPAR x f_{esc} (Badgley et al., 2017). NIRv from moderate spectral resolution satellite imagery and field spectrometers has been shown to track GPP and SIF at monthly to seasonal timescales presumably because changes in canopy structure influence light capture and these changes coincide with changes in GPP (Badgley et al., 2019; Badgley et al., 2017; Dechant et al., 2020). FCVI is also a proxy for fPAR x f_{esc}, but derived from radiative transfer theory, rather than an empirical relationship (Yang et al., 2020). FCVI is calculated from RS data by subtracting the reflectance in the NIR from the reflectance in the visible range. FCVI was demonstrated to capture the canopy structure and radiation components of the SIF signal, which tracked SIF and GPP, yet showed differences from NIRv due to exposed soil within the vegetated study areas. In previous studies, FCVI and NIRv were similar for dense green canopies where soils have less of an impact, but this has not yet been tested in the tropics (Wang et al., 2020; Badgley et al., 2019; Dechant et al., 2020). NIRvrad was proposed as a proxy for GPP on half-hourly and daily timescales, in contrast to NIRv and FCVI which track changes on longer timescales (Wu et al., 2020; Dechant et al., 2020; Baldocchi et al., 2020; Zeng et al., 2019). NIRvrad is calculated by multiplying NDVI by the NIR radiance. Because the radiance of NIR accounts for incoming radiation at these short timescales, NIRvrad demonstrated the ability to track GPP and SIF on half-hourly and diurnal scales as well as seasonally (Dechant et al., 2020; Baldocchi et al., 2020; Zeng et al., 2019; Wu et al., 2020).

These emerging quantities, NIRv, FCVI, and NIRvrad, have advantages over RIs when making inferences about productivity and have practical advantages over making SIF measurements. Because they exploit additional information from the NIR region of the spectrum, NIRv, FCVI, and NIRvrad do not saturate in dense canopies or suffer the same level of contamination from dead vegetation and soils as traditional RIs (Baldocchi et al., 2020; Badgley et al., 2017). Yet, NIRv, FCVI, and NIRvrad are similarly straightforward to measure and calculate as RIs, which is advantageous over making and interpreting SIF measurements requiring very high spectral resolution and

https://doi.org/10.5194/bg-2021-95
Preprint. Discussion started: 19 April 2021

multiple instruments. Furthermore, readily available UAS-based hyperspectral sensors are capable of robust measurements of NIRv, FCVI, and NIRvrad on the scale of tens of centimeters, but there are not yet hyperspectral imagers with sufficient spectral resolution to retrieve the SIF signal available on UAS platforms due to payload limitations. For these reasons, NIRv, FCVI, and NIRvrad can be used as a compliment to SIF by decoupling the structural component of the SIF signal or, as an efficient and accessible measurement of structure and light regime, can serve as proxies for GPP or SIF or APAR, for instance.

Unmanned aerial systems (UAS)-based instruments have the capability of capturing information at ultra-high spatial scales, i.e. in tens of centimeters. In this regard, UAS-based data have the potential to improve our understanding of spectral vegetation indicators, tropical forest canopy structure, and the light capture and scatter regime over a range of scales that are poorly resolved by other remote sensing platforms.

Here we use high spatial resolution UAS measurements to evaluate spatial and temporal variation in a tropical forest canopy and compare commonly used spectral indices (NDVI and EVI) to newer vegetation indicators (NIRv, NIRvrad, and FCVI) by (i) examining correlations between GPP and vegetation indicators using mean values across the canopy throughout the day, (ii) evaluating the distribution of fine spatial resolution values (~15 cm) across the canopy and examining changes in this spatial variation throughout the course of two days, and finally (iii) examining varying spatial scales and identifying the dominant spatial scale driving variation across our 10 ha study region.

2 Materials and Methods

2.1 Study Area

Barro Colorado Island (BCI), Panama, is a 1560 ha island (approximately 15 km^2) in Gatun Lake, which was formed by the construction of the Panama Canal. The Smithsonian Tropical Research Institute manages the preserved area specifically for research. This semi-deciduous moist tropical forest receives approximately 2640 mm mean annual precipitation and has a mean temperature of 26^{o}C with a dry season from approximately January through April (Detto et al., 2018). There is high species diversity, with approximately 500 tree species, approximately 60 species per ha, and about 6.3% of trees at >30cm diameter at breast height (dbh) (Bohlman and O'brien, 2006; Condit et al., 2000). The UAS and ground measurements were focused on an area approximately 10 ha within the footprint of an eddy covariance tower near the center of the island (9.156440°, -79.848210°).

2.2 Data collection

The GatorEye Unmanned Flying Laboratory is a hardware and software system built for sensor fusion applications, and which includes hyperspectral, thermal, and visual cameras and a Lidar sensor, coupled with a differential GNSS, internal hard drives, computing systems, and an Inertial Motion Unit (IMU). Hardware and processing details, as well as data downloads, are available at www.gatoreye.org. The GatorEye flew 13 missions on January 30 and 31, 2019 over the forest canopy within the eddy covariance tower footprint at an average height of 120

https://doi.org/10.5194/bg-2021-95
Preprint. Discussion started: 19 April 2021

m above ground level (AGL) and at 12 m/s. In this study, we used radiometrically calibrated flight transects from the Nano VNIR 270 spectral band hyperspectral sensor (Headwall Photonics, Fitchburg, MA, USA) which covered approximately 1 ha per flight within the EC footprint in this study. The Nano spectrally samples at approximately 2.2 nm and 12-bit radiometric resolution from 400 to 1050 nm. The frame rate was set to 100 fps, with an integration time of 12 ms. and provided a pixel resolution of approximately 15x15 cm. The Nano was calibrated to radiance by the manufacturer before the field campaign and pixel drift was removed by dark images collection, which was corrected for during the conversion from digital number to radiance. The hyperspectral transects were equally subset for each flight in ENVI + IDL (Harris Geospatial, Boulder, CO). Each flight resulted in 1920 transects of approximately 400 m length composing three blocks discretized in 2500 data points. Simultaneous lidar was collected using a VLP-32c ultra puck (Velodyne, San Jose, CA), which was processed to a 0.5x0.5 m resolution digital surface model (DSM).

Turbulent fluxes and meteorological variables were measured from a 40 m Eddy Covariance (EC) flux tower. The eddy covariance system includes a sonic anemometer (CSAT3, Campbell Scientific, Logan, UT) and an open-path infrared CO_2/H_2O gas analyzer (LI7500, LiCOR. Lincoln, NE). High-frequency (10Hz) measurements were acquired by a datalogger (CR1000, Campbell Scientific) and stored on a local PC. Other measurements made at the tower include air temperature and relative humidity (HC2S3, Rotronic, Hauppauge New York), photosynthetically active radiation (PAR; BF5, Delta-T Devices, UK). EC data were processed with a custom program using a standard routine described in Detto et al. (2010). GPP was derived from daytime values of NEE by adding the corresponding mean daily ecosystem respiration obtained as the intercept of the light response curve (Lasslop et al., 2010). Flux data was available for only January 31.

An HH2 Pro Spectroradiometer (HH2; ASD/Panalytical/Malvern, Boulder, CO) fitted with a diffuse cosine receptor was used on the ground in full sun at the forest edge to record incoming irradiance on January 30 and 31, 2019 (~ 3nm FWHM and spectral sampling at 1nm). HH2 irradiance was resampled to match the Nano hyperspectral sensor and used to calculate reflectance. A calibrated reference tarp was placed in full sun at the forest edge and the UAS flew over and recorded the tarp each UAS flight. Reflectance was calculated separately using the HH2 and tarp data and resulting reflectance values compared as a method to vicariously cross-calibrate reflectance from the hyperspectral data (<7.0% difference for all data in the study). In addition, PAR was calculated with the HH2 data and compared to the tower-mounted PAR measurement (approximately 1.5 km apart) to help understand any differences in the sky conditions during flight times. PAR differences across the site for each flight time for the duration of flights (approximately 10-15 minutes in length each) ranged between 4.0% and 10.3%.

2.3 Vegetation indicators

We calculated NDVI and EVI as (Huete et al., 2002; Rouse Jr et al., 1974):

$$NDVI = \frac{R_{770-800} - R_{630-670}}{R_{770-800} + R_{630-670}} \tag{3}$$

https://doi.org/10.5194/bg-2021-95
Preprint. Discussion started: 19 April 2021

$$EVI = \frac{2.5(R_{770-800} - R_{630-670})}{R_{770-800} + 6 \times R_{630-670} - 6 \times R_{460-475} + 1} \quad (4)$$

where we used the averages of 770-800 nm for NIR, 630-670 nm for red, and 460-475 nm for blue bands to reduce noise.

We calculated the near-infrared vegetation index NIRv as:

$$NIRv = NDVI \times R_{770\text{-}800} \quad (5)$$

where R770-800 is the NIR reflectance (Badgley et al., 2017).

The fluorescence correction vegetation index (FCVI) was calculated from spectral data by subtracting the reflectance in the visible range (R400-700) from the NIR reflectance (Yang et al., 2020) as follows

$$FCVI = R_{770\text{-}800}\text{-}R_{400\text{-}700} \quad (6).$$

The near-infrared radiance of vegetation (NIRvrad) was calculated similarly to the NIRv, except NDVI was multiplied by the radiance, rather than reflectance, from the NIR region (Rad770-800) (Wu et al., 2020) as follows:

$$NIRvrad = NDVI \times \mathrm{Rad}_{770\text{-}800} \quad (7).$$

2.4 Data Analysis

We examined mean values across the canopy over the course of one day by creating diurnal time series scatterplots for the tower-based PAR data, tower-based GPP data, and means of all spectral vegetation indicators, on Jan 31, 2019, and ran comparisons using Pearson's correlation coefficients to examine correlations. At fine spatial scales, i.e. pixel level of ~15 cm, we created density plots, calculated the coefficient of variation (CV), and calculated the means of all vegetation indicators (NIRv, FCVI, NIRvrad, NDVI, EVI) for each flight to compare spatial and temporal variability. To determine which spatial scales dominate the variability of each vegetation quantity, we ran power spectrum wavelet analysis using code created in the Matlab programming language (Mathworks, Natick, Massachusetts). For each vegetation quantity and each flight, and for the lidar elevation model representing canopy height, we computed the Morlet wavelet power spectrum of individual transects (Torrence and Compo, 1998). All power spectra from the wavelet analysis were normalized to unit variance. An ensemble power spectrum for each vegetation indicator was created by averaging across all the transects of each flight and then across flights. We then compared the power spectra for each vegetation indicator and lidar data to compare the spatial scales at which the quantities captured variability as well as the spatial scale at which the lidar-based elevation model captured variability. For illustration purposes, Fig. S3 is an example of two signals, a higher and lower noise signal created with fractals (Signal A and B, respectively, Fig. A1) and the corresponding power spectra which decay differently at smaller spatial scales (Power Spectra, Fig. A1). Initial UAS data processing was carried out in Interactive Data Language (IDL) and Environment for Visualizing Images (ENVI) (Harris Geospatial, Boulder, CO). Other analysis, including graphical illustrations, were carried out using the R open source environment with libraries dplyr, ggplot, and tidyverse (R Development Core Team, 2010; Wickham et al., 2018; Wickham, 2017, 2016) and Matlab (Mathworks, Natick, Massachusetts).

https://doi.org/10.5194/bg-2021-95
Preprint. Discussion started: 19 April 2021

Biogeosciences
Discussions

3 Results and discussion

3.1 Diurnal trend in spectral quantities, PAR, and GPP

The degree to which remote sensing vegetation indicators represent changes in GPP depend largely on canopy structure-dependent light absorption and scattering processes, thus a joint relationship between a remote sensing vegetation quantity, PAR, and GPP. Fig. 1 shows GPP, PAR, and the mean value of each vegetation quantity at each flight time over the course of January 31, the day on which we had overlapping data (Fig. 1a-d). Additionally, Pearson correlation coefficients among mean NIRv, FCVI, NIRvrad, EVI, and NDVI for each flight time and the GPP and PAR values at the flight times are shown in Fig. 1d. NIRv is significantly and strongly positively correlated to both FCVI ($r=0.9$, $p<0.001$) and EVI ($r=0.9$, $p<0.01$). NIRvrad is the only vegetation quantity with a significant correlation to PAR and GPP, with a strong positive relationship (0.9 and 0.81, respectively, p-values <0.05; Fig. 1d) and mean NIRvrad values have the greatest relative diurnal change among the vegetation indicators (Fig. 1c and d). These results demonstrate that a shared correlation of NIRvrad and GPP to PAR results in mean NIRvrad tracking diurnal changes in GPP to a greater degree than NIRv, FCVI, NDVI or EVI, because NIRvrad takes incoming radiation into account whereas the other vegetation indicators do not. This evidence supports the proposed use of NIRvrad as a proxy for changes in GPP on short timescales and as a more efficient measurement in the sense that a separate instrument to measure PAR is not needed (Wu et al., 2020; Zeng et al., 2019).

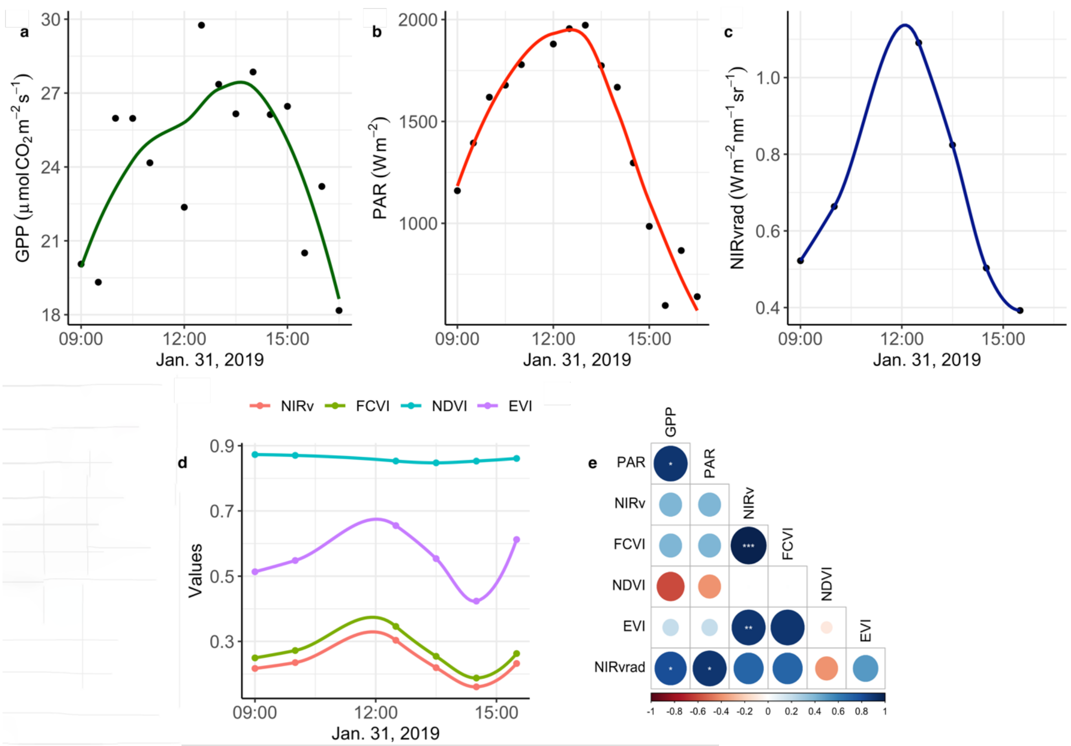

Fig. 1. Diurnal time series of a) GPP b) PAR c) NIRvrad d) NIRv, FCVI, NDVI, and EVI e) comparisons of quantities using Pearson correlations color indicates strength of relationship, * = p-value<0.05, ** = p-value <0.01, *** = p-value <0.001.

https://doi.org/10.5194/bg-2021-95
Preprint. Discussion started: 19 April 2021

3.2 Tropical forest canopy variation

Spatial distributions of all pixels and CV of NIRv, FCVI, and NIRvrad are similar to one another and show considerable variation spatially across the canopy and temporally over the course of a day and across days (Fig. 2a-c, Table A2). We show for the first time that NIRv and FCVI are virtually the same in this dense tropical forest due to both similarly representing fPAR x f_{esc} in conditions of little background soil, supporting the predictions of earlier studies (Dechant et al., 2020; Zeng et al., 2019; Yang et al., 2018b; Wu et al., 2020). NIRv, FCVI, and NIRvrad distributions are distinct from EVI and NDVI (Fig. 2a-e, Table A2, and Table A2). NIRv, FCVI, and NIRvrad have the highest CV at each flight time (between 39.78% and 91.54%, Table A1), followed by EVI (between 20.24% and 37.24%, Table A2) and NDVI had the least variation at any flight time (between 9.83% and 12.82%, Table A2). During morning and afternoon hours, mean values across the canopy fail to capture extreme high (NIRv, NIRvrad, and FCVI) or low values (NDVI) for some indices. This pattern suggests "hot" and "cool" spots of activity related to heterogeneity in forest structure and low sun angles. In previous studies, the directional effects on NIRv have been examined on coarse spatial scales (i.e. satellites) and have been proposed as an area of need for improving NIRv agreement to GPP or as a potential tool to normalize SIF for these effects to improve SIF agreement to GPP (Hao et al., 2021; Dechant et al., 2020; Baldocchi et al., 2020; Zhang et al., 2020). Our results demonstrate that UAS-based data are suitable for normalizing SIF at high spatial resolution in addition to recording structural heterogeneity of a tropical forest. The higher variability of NIRv, FCVI, and NIRvrad, suggest they may have the ability to best represent the structural heterogeneity of the tropical forest canopy, followed by EVI and then NDVI (Fig. 2a-e). Because NIRv and NIRvrad use NDVI, these results also indicate that including the NIR reflectance or NIR radiance is the largest contributing factor in this variability (Fig. 2a, c, and e). EVI variability was higher than NDVI, but lower than that of NIRv, FCVI, and NIRvrad, indicating that EVI has a different level of sensitivity to components of the canopy, viewing geometry, and light absorption and scattering regime of the canopy than the other quantities (Table A1and Table A2).

Midday distributions of NIRv, FCVI, and NIRvrad on Jan. 30 at 12:00 and 1330 and Jan. 31 at 12:30 are less skewed than at other times whereas morning and afternoon distributions are skewed toward lower values, except for Jan. 31 at 15:30 (Fig. 2a-c). On both days, when mean values peak at midday, the variation for all vegetation indicators is lowest (Jan 30, 1200 CV between 47.6 and 49.2 and Jan 31, 1230 CV between 45.6 and 47.2) (Fig. 2, Table A1). The highest variability occurred in the afternoon on both days (Jan 30, 1630 CV between 91.3% and 91.5 and Jan 31, 1430 CV between 83.3% and 83.8% for all quantities) (Fig. 2, Table A2). The low variability of NIRv, FCVI, and NIRvrad and high means at midday indicates that viewing and sun geometry drive the higher- and lower- values during morning and afternoon and this effect is greater in the afternoon than the morning (Fig. 2, Table A2). However, a different pattern is apparent on Jan. 31 during the 1530 flight time when mean values increased from the 1430 means and the CV values were the lowest of any flight observations in the study. It is possible that this was due to another type of effect on illumination geometry, such as wind influencing the UAS, some diffuse radiation effects, or hotspot effects. The effect appears to have a greater relative influence on EVI, thus changing the viewing angle to record greater understory captured by the blue reflectance could be possible.

https://doi.org/10.5194/bg-2021-95
Preprint. Discussion started: 19 April 2021

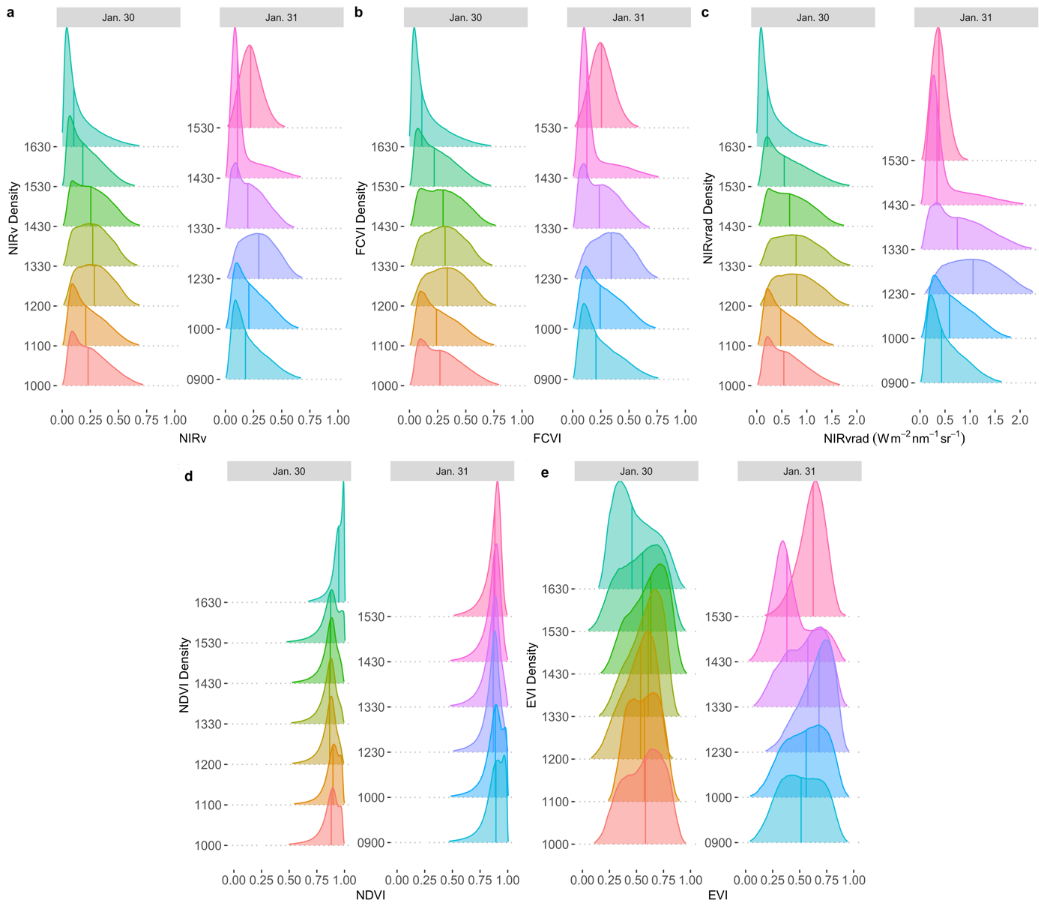

Fig. 2. NIRv (a), FCVI (b), and NIRvrad (c) density plots for each flight time on January 30, 2019 (column 1each panel) and January 31 (column 2 each panel). Colours of distributions indicate the flight time and day.

3.3 Power Spectrum Analysis

Power spectrum analysis was used to identify the dominant spatial scales driving variability across the canopy (Fig. 3), where the area beneath the curve is proportional to the variance because it is the spectrum divided by the corresponding scale and then plotted as a function of the log of the scale (Example signals and power spectra provided in Fig. A1). Consistent with predictions in previous studies, NIRvrad and FCVI are indistinguishable in their spatial variability (Fig. 3) (Dechant et al., 2020; Zeng et al., 2019). Power spectrum analysis shows a strong peak around 50 m spatial scale for NIRv, NIRvrad, FCVI, and EVI, whereas NDVI peaks at approximately 90 m. The largest tree crown sizes on BCI are on the order of 20-30 m in diameter and the most common crown sizes are between 4-10 m (Fig. A2). Thus, the spatial variability of the vegetation indicators is strongly influenced by larger forest structures, such as forest gaps and tree clusters, rather than individual tree crowns. This is also confirmed by the power spectrum of the lidar-derived canopy surface model, which displays a peak at 70 m scale, indicating that larger than tree crown scales produce the most variability in canopy height. In other words, UAS-based lidar data also show that canopy

https://doi.org/10.5194/bg-2021-95
Preprint. Discussion started: 19 April 2021

heights are more similar in one area at about 70 m. This demonstrates that trees with similar spectral response at similar heights occur in groups in this forest, or at least the tree clusters, i.e. larger forest structures are the smallest regularly detectible unit. Therefore, the vegetation indicators are less effective in capturing differences among leaves, clumping leaves, or among the most frequent tree crown sizes on BCI (4-10 m according to stereograph photo measured sunlit tree crown sizes; Fig. A2). However, note how the peak in the vegetation indicators are broader than the peak in the lidar data, suggesting smaller scales are still contributing to the total spatial signal. NDVI displays a different shape with a slower decay at small scales, indicating less distinguishable spatial structures, and a peak shifted to the larger scales (Fig. 3). At much larger scales (>100-200 m), the vegetation indicators decline smoothly, while NDVI and especially lidar show an increase in variance probably associated with topographic heterogeneity.

One reason why vegetation indicators and LiDAR captured variability at spatial scales larger than the most common tree crown sizes on BCI is that canopy heights tend to be more uniform on BCI compared to other tropical forests, possibly due to wind (Bohlman and O'brien, 2006). For example, Dipterocarpus dominated South-East Asian forests have emergent trees that can reach up to 60 m in height. Additionally, tree crowns on BCI tend to be more flat-topped than conical or rounded, and trees can be found clumped in similar heights, which could explain why the most often detected unit is larger than the mean of a single crown. On the other end of the spectrum, forest gaps can be larger than a single crown because treefall often affects neighbouring trees.

Vegetation indicators and the LiDAR-derived surface model represent the spectral and structural properties most broadly of the upper canopy, and thus it is conceivable that they display similar spatial variability. However, NIRv, FCVI, NIRvrad, and EVI discriminated details at a different spatial scale from NDVI and LiDAR. These results parallel the variability detected in their distributions (Fig. 2 and Table A1), where NDVI was most different from the other vegetation indicators. Taken together, these results show that NIRv, FCVI, and NIRvrad have a smoother spatial pattern and peak at finer scales than NDVI, thus, these indicators would serve as finer resolution indicators of spatial heterogeneity and more adept to monitor changes in structure of the canopy than NDVI. The emerging indicators may be finer scale proxies for GPP than NDVI and can potentially disaggregate the physiological and structural component of SIF when SIF measurements are available since changes in structure of the forest coincide with changes in GPP. Emerging indicators' heightened ability to differentiate canopy is likely due to the influence of high upwelling of NIR from the canopy and understory, particularly in the dry season, for which tend to blur the signal of the upper canopy for NDVI. Notably, EVI and NDVI, two common indicators of vegetation greenness, show differences in their power spectrum, in particular the slope of the curve for scales less than 20 m. EVI was designed to better capture vegetation changes by exploiting variability in the reflectance in the blue range, especially effective in dense green canopies. This may help explain the scale of variability in this canopy where variation in the blue may be expected to manifest, especially because deciduous crowns are present on BCI.

https://doi.org/10.5194/bg-2021-95
Preprint. Discussion started: 19 April 2021

Biogeosciences
Discussions

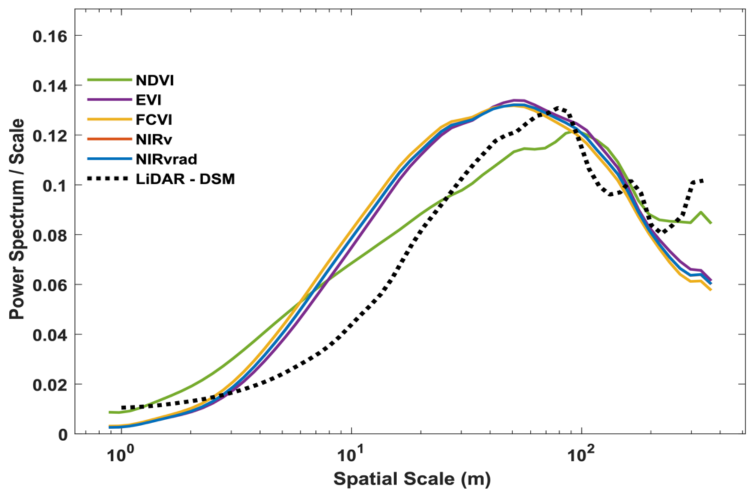

Fig. 3. Ensemble wavelet power spectra for all the quantities used in this study and a LiDAR-derived digital surface model (DSM). Note that FCVI and NIRv are similar, thus the NIRv curve is obscured by the FCVI. Ensembles were created by averaging the spectrum of individual transects, then averaging across flights. Note that in this representation, the spectrum divided by the corresponding scale as a function of the log of the scale, the area beneath the curve is proportional to the variance.

4 Conclusions

Presented here for the first time are NIRv, FCVI, and NIRvrad, emerging vegetation indicators related to fPAR and the scattering of SIF photons, of a tropical forest canopy calculated using UAS-based hyperspectral data. This study demonstrates several advantages to using these emerging vegetation indicators, as well as high spatial resolution observations to improve our understanding of tropical forest structure and coincident functional changes. Our findings demonstrate mean values of NIRvrad track GPP over the course of a day because of a shared correlation among NIRvrad, PAR, and GPP, making NIRvrad a potential proxy for tracking GPP on short timescales without the need for separate measurements of incoming irradiance. Also, NIRv, FCVI, and NIRvrad at high spatial resolution (~15cm) unveil greater spatial and diurnal variability of BCI's tropical forest canopy versus EVI or NDVI, exposing fine-scale structural heterogeneity underlying coarser scale measurements that may pave the way to improve our understanding of the relationship between GPP and remote sensing observations. The dominant scale driving spatial variability of spectral measurements and lidar data are larger forest structures occurring on BCI, such as groups of similar trees or forest gaps. Yet, NIRv, FCVI, NIRvrad, and EVI's smaller, broader peaks indicate these four indices incorporate smaller scale information more completely than NDVI, demonstrating the efficacy of using NIRv, FCVI, NIRvrad, and EVI to record and track structure of vegetation. Taken together, the demonstrated ability to track GPP, expose heterogeneity and variability effectively, and capture specific forest structure characteristics of BCI open greater possibilities to examine and compare structure within and across this tropical forest. Additionally, while this study focuses on BCI, these techniques could have global implications by applying more broadly for the purposes of defining

https://doi.org/10.5194/bg-2021-95
Preprint. Discussion started: 19 April 2021

structures, tracking structural changes, monitoring coincident changes in GPP or microclimates, disaggregating SIF signals, or as inputs to models of tropical forest structure and function.

Because remote sensing advancements are making it possible to capture physiological responses of vegetation, the importance of improved techniques to examine the radiation regime, for instance estimating fPAR or APAR, can be overlooked. However, recent studies have highlighted the importance and difficulties of measuring fPAR and APAR, the strong dependence of measurements such as SIF on illumination and viewing geometry, SIF escape potential, as well as the need for increased understanding of structure-related radiation regime information more generally e.g. (Hao et al., 2021; Dechant et al., 2020; Baldocchi et al., 2020; Rocha et al., 2021; Zhang et al., 2020). For NIRv, FCVI, and NIRvrad, inclusion of the NIR spectral region makes the emerging indices more sensitive to incoming, absorbed, and scattered radiation, and in the sense of remote sensing vegetation measurements, this includes changing illumination and viewing geometry, changes in canopy leaf angles or associated structure changes. In the case of NIRvrad, which was most strongly associated with GPP, these changes can even be captured diurnally. This punctuates the importance of understanding the incoming solar radiation, absorbed and scattered radiation, and illumination and viewing geometry of any remote sensing data, but it also encourages exploiting such observations to improve our ability to measure structure-related light capture and scattering patterns. It is in this role, we show these measurements are valuable tools to improve our understanding of complex vegetation surfaces, may be used to separate the components of a SIF signal, or used directly as an improved estimate of fPAR, APAR, or GPP and do so with more straightforward instrumentation and processing than SIF, for instance.

https://doi.org/10.5194/bg-2021-95
Preprint. Discussion started: 19 April 2021

Biogeosciences Discussions Open Access EGU

349 # 5 Appendix

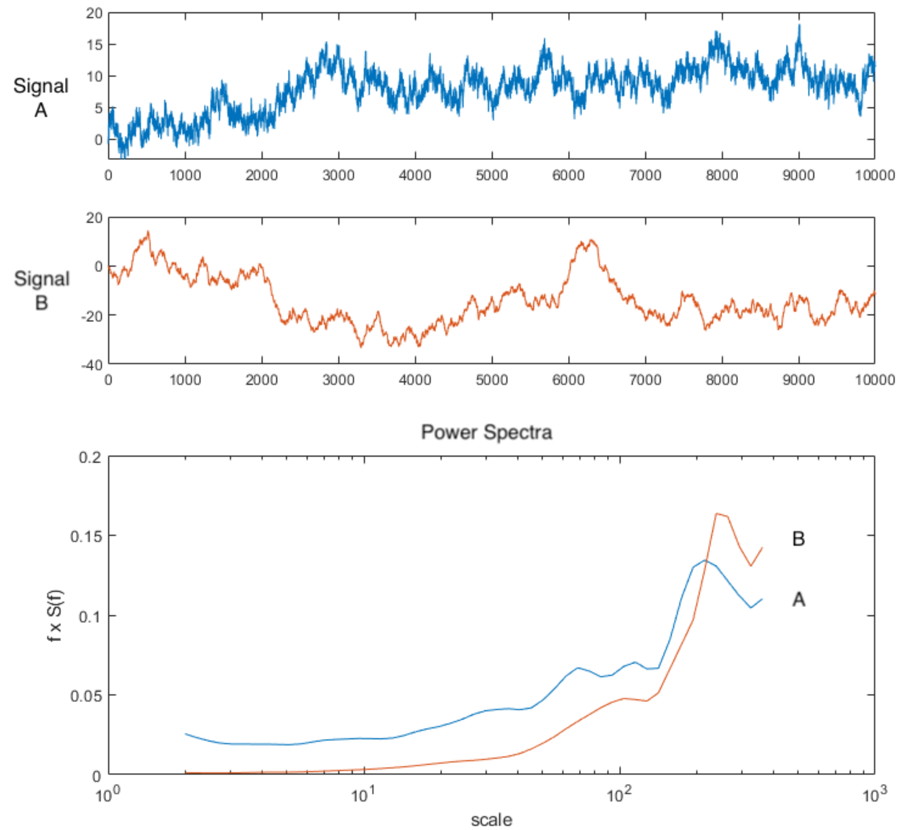

350

351 **Figure A1.** **Sample signals with relatively higher noise (Signal A) and lower noise (Signal B) and their corresponding**
352 **Power Spectra ensemble plotted as normalized on log scale. Note the representation of the variance by area under the curve**
353 **is preserved by multiplying the Power (S(f)) by the frequency (f). In this way the area beneath the curve is still proportional**
354 **to the variance.**

355

https://doi.org/10.5194/bg-2021-95
Preprint. Discussion started: 19 April 2021

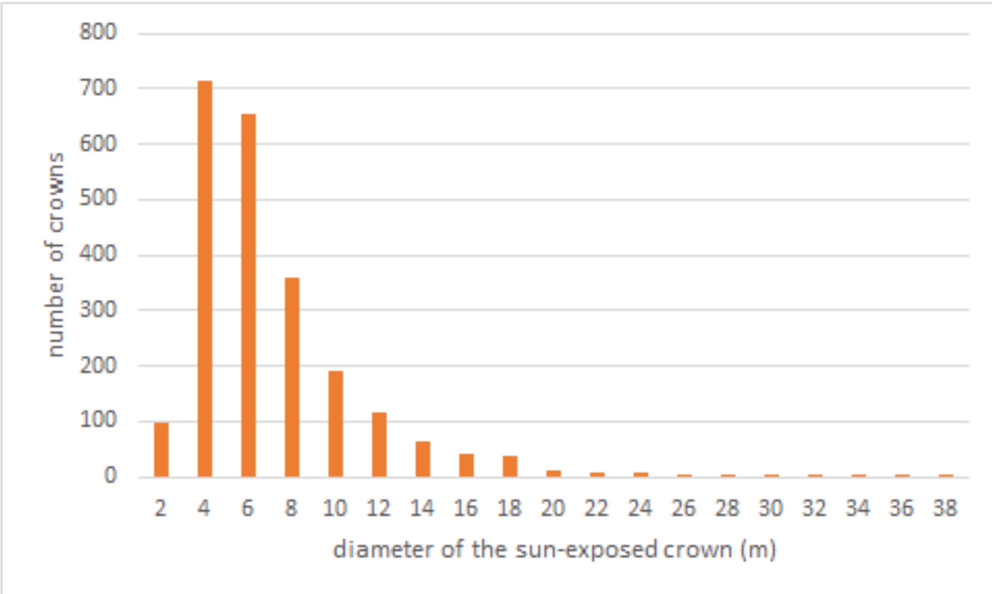

Figure A2. **Distribution of tree crown sizes on BCI in a sample ~10 ha plot taken from digitized high spatial resolution stereo photos that were linked to stems in the field. This ~10 ha plot does not coincide with the ~10 ha area sampled by the UAS near the eddy covariance tower in this study. Figure: Stephanie Bohlman.**

Table A1. Mean, standard deviation (Sdev) and coefficient of variation (CV) of NIRv, NIRvrad, and FCVI measurements for the study.

Flight Time	Mean NIRv	SDev NIRv	CV NIRv (%)	Mean NIRvrad	SDev NIRvrad	CV NIRvrad (%)	Mean FCVI	SDev FCVI	CV FCVI (%)
Jan30_1000	0.26	0.16	61.36	0.60	0.36	60.54	0.29	0.18	59.69
Jan30_1100	0.24	0.15	61.48	0.54	0.33	60.56	0.27	0.16	60.89
Jan30_1200	0.29	0.15	49.20	0.82	0.39	47.59	0.34	0.16	47.88
Jan30_1330	0.28	0.14	50.46	0.81	0.40	49.24	0.32	0.16	49.16
Jan30_1430	0.27	0.15	55.46	0.70	0.38	54.38	0.31	0.17	54.22
Jan30_1530	0.21	0.14	65.10	0.63	0.41	64.71	0.25	0.16	64.01
Jan30_1630	0.16	0.14	91.54	0.32	0.30	91.54	0.17	0.15	91.39
Jan31_0900	0.22	0.14	66.31	0.52	0.34	65.25	0.25	0.16	66.01
Jan31_1000	0.24	0.14	59.43	0.66	0.39	58.29	0.27	0.16	59.04
Jan31_1230	0.30	0.14	47.17	1.09	0.50	45.63	0.35	0.16	45.91
Jan31_1330	0.22	0.14	61.91	0.82	0.51	61.47	0.25	0.15	60.53
Jan31_1430	0.16	0.14	85.32	0.50	0.42	83.81	0.19	0.16	83.83

Jan31_1530	0.86	0.08	9.83	0.61	0.12	20.24	0.53	0.04	8.15

Table A2. Mean, standard deviation (Sdev) and coefficient of variation (CV) of NDVI and EVI measurements for the study.

Flight Time	Mean NDVI	SDev NDVI	CV NDVI (%)	Mean EVI	SDev EVI	CV EVI (%)
Jan30_1000	0.86	0.10	11.64	0.57	0.18	31.54
Jan30_1100	0.88	0.09	10.15	0.57	0.14	24.40
Jan30_1200	0.85	0.09	10.38	0.52	0.15	28.48
Jan30_1330	0.85	0.09	10.60	0.59	0.15	25.24
Jan30_1430	0.85	0.09	10.35	0.61	0.16	26.84
Jan30_1530	0.85	0.11	12.52	0.54	0.19	35.21
Jan30_1630	0.93	0.06	6.69	0.49	0.18	36.90
Jan31_0900	0.87	0.10	11.54	0.51	0.19	37.24
Jan31_1000	0.87	0.10	11.08	0.55	0.19	34.66
Jan31_1230	0.85	0.08	9.82	0.66	0.15	22.72
Jan31_1330	0.85	0.09	10.70	0.55	0.19	33.80
Jan31_1430	0.85	0.09	10.58	0.42	0.18	43.07
Jan31_1530	0.86	0.08	9.83	0.61	0.12	20.24

Code availability

Data availability

GatorEye data related to this project can be downloaded from www.gatoreye.org. Code and other material with links provided upon request (repository forthcoming).

Author contributions

T.M. designed the study with the help of S.P. and S.A.B.. M.D. and T.M. outfitted the tower and collected tower-based data, T.M. and E.N.B. collected the UAS data. E.N.B., A.M.A.Z., and T.M. pre-processed the hyperspectral and lidar data. T.M. and M.D. further processed UAV, lidar, and GPP data and ran data analysis. M.D., S.P., S.A.B., C.S., contributed with the methodological framework, data processing analysis and write up T.M., M.D., S.P., S.A.B., C.S.,.

E.N.B., and A.M.A.Z. contributed to the interpretation, quality control and revisions of the manuscript. All authors read and approved the final version of the manuscript.

Competing interests

The authors declare no conflict of interest.

Acknowledgments

Support for this project, including portions of field logistic and data collection costs and materials, and support for T.M., was provided by the Provost's Postdoctoral Fellows Program at Florida State University. E.N.B. was supported through the School of Forest Resources and Conservation, A.M.A.Z through the Center for Latin American Studies, and hardware, software, and system costs associated with the GatorEye and data collection were provided through the McIntire Stennis Program of the USDA and the School of Forest Resources and Conservation. M.D. was supported by the Carbon Mitigation Initiative at Princeton University. The authors wish to thank the vast support of the collaborators, staff, and researchers at the Smithsonian Tropical Research Institute and, specifically at Barro Colorado Island, without which this research would not be possible. Among other contributors to the work, we also extend special thanks to Alfonso Zambrano, Carli Merrick, Riley Fortier, and Pete Kerby-Miller for field work assistance, and Dr. S. Joseph Wright and Dr. Helene Muller-Landau for support on site as well.

References

Alonso, L., Moreno, J., Moya, I., and R. Miller, J. R.: A Comparison of Different Techniques for Passive Measurement of Vegetation Photosynthetic Activity: Solar-Induced Fluorescence, Red-Edge Reflectance Structure and Photochemical Reflectance Indices, IEEE, 3, 2003.

Alonso, L., Gómez-Chova, L., Vila-Francés, J., Amorós-López, J., Guanter, L., Calpe, J., and Moreno, J.: Sensitivity analysis of the Fraunhofer Line Discrimination method for the measurement of chlorophyll fluorescence using a field spectroradiometer, IEEE, 4, 2007.

Alonso, L., Gómez-Chova, L., Vila-Francés, J., Amorós-López, J., Guanter, L., Calpe, J., and Moreno, J.: Improved Fraunhofer Line Discrimination Method for Vegetation Fluorescence Quantification, IEEE GEOSCIENCE AND REMOTE SENSING LETTERS, 5, 5, 2008.

Badgley, G., Field, C. B., and Berry, J. A.: Canopy near-infrared reflectance and terrestrial photosynthesis, Sci Adv, 3, e1602244, 10.1126/sciadv.1602244, 2017.

Badgley, G., Anderegg, L. D. L., Berry, J. A., and Field, C. B.: Terrestrial gross primary production: Using NIRV to scale from site to globe, Glob Chang Biol, 25, 3731-3740, 10.1111/gcb.14729, 2019.

Baldocchi, D. D., Ryu, Y., Dechant, B., Eichelmann, E., Hemes, K., Ma, S., Rey Sanchez, C., Shortt, R., Szutu, D., Valach, A., Verfaillie, J., Badgley, G., Zeng, Y., and Berry, J. A.: Outgoing Near Infrared Radiation from Vegetation Scales with Canopy Photosynthesis Across a Spectrum of Function, Structure, Physiological Capacity and Weather, Journal of Geophysical Research: Biogeosciences, 10.1029/2019jg005534, 2020.

Bohlman, S. and O'Brien, S.: Allometry, adult stature and regeneration requirement of 65 tree species on Barro Colorado Island, Panama, Journal of Tropical Ecology, 22, 123-136, 10.1017/s0266467405003019, 2006.

Castro, A. O., Chen, J., Zang, C. S., Shekhar, A., Jimenez, J. C., Bhattacharjee, S., Kindu, M., Morales, V. H., and Rammig, A.: OCO-2 Solar-Induced Chlorophyll Fluorescence Variability across Ecoregions of the Amazon Basin and the Extreme Drought Effects of El Niño (2015–2016), Remote Sensing, 12, 10.3390/rs12071202, 2020.

https://doi.org/10.5194/bg-2021-95
Preprint. Discussion started: 19 April 2021

Clark, D. A., Asao, S., Fisher, R., Reed, S., Reich, P. B., Ryan, M. G., Wood, T. E., and Yang, X.: Reviews and syntheses: Field data to benchmark the carbon cycle models for tropical forests, Biogeosciences, 14, 4663-4690, 10.5194/bg-14-4663-2017, 2017.

Cogliati, S., Verhoef, W., Kraft, S., Sabater, N., Alonso, L., Vicent, J., Moreno, J., Drusch, M., and Colombo, R.: Retrieval of sun-induced fluorescence using advanced spectral fitting methods, Remote Sensing of Environment, 169, 344-357, 10.1016/j.rse.2015.08.022, 2015.

Condit, R. S., Watts, K., Bohlman, S., Perez, R., Foster, R. B., and Hubbell, S. P.: Quantifying the deciduousness of tropical forest canopies under varying climates, Journal of Vegetation Science, 11, 10, 2000.

Dechant, B., Ryu, Y., Badgley, G., Zeng, Y., Berry, J. A., Zhang, Y., Goulas, Y., Li, Z., Zhang, Q., Kang, M., Li, J., and Moya, I.: Canopy structure explains the relationship between photosynthesis and sun-induced chlorophyll fluorescence in crops, Remote Sensing of Environment, 241, 10.1016/j.rse.2020.111733, 2020.

Detto, M., Baldocchi, D., and Katul, G. G.: Scaling Properties of Biologically Active Scalar Concentration Fluctuations in the Atmospheric Surface Layer over a Managed Peatland, Boundary-Layer Meteorology, 136, 407-430, 10.1007/s10546-010-9514-z, 2010.

Detto, M., Wright, S. J., Calderon, O., and Muller-Landau, H. C.: Resource acquisition and reproductive strategies of tropical forest in response to the El Nino-Southern Oscillation, Nature communications, 9, 913, 10.1038/s41467-018-03306-9, 2018.

Frankenberg, C., Fisher, J. B., Worden, J. R., Badgley, G., Saatchi, S. S., Lee, J. E., Toon, G. C., Butz, A., Jung, M., Kuze, A., and Yokota, T.: New global observations of the terrestrial carbon cycle from GOSAT: Patterns of plant fluorescence with gross primary productivity, Geophysical Research Letters, 38, 10.1029/2011gl048738, 2011.

Gamon, J. A., Kovalchuck, O., Wong, C. Y. S., Harris, A., and Garrity, S. R.: Monitoring seasonal and diurnal changes in photosynthetic pigments with automated PRI and NDVI sensors, Biogeosciences, 12, 4149-4159, 10.5194/bg-12-4149-2015, 2015.

Gao, W., Kim, Y., Ustin, S. L., Huete, A. R., Jiang, Z., and Miura, T.: Multisensor reflectance and vegetation index comparisons of Amazon tropical forest phenology with hyperspectral Hyperion data, Remote Sensing and Modeling of Ecosystems for Sustainability IV, 10.1117/12.734974, 2007.

Glenn, E. P., Huete, A. R., Nagler, P. L., and Nelson, S. G.: Relationship Between Remotely-sensed Vegetation Indices, Canopy Attributes and Plant Physiological Processes: What Vegetation Indices Can and Cannot Tell Us About the Landscape, Sensors, 8, 24, 2008.

Guanter, L., Frankenberg, C., Dudhia, A., Lewis, P. E., Gómez-Dans, J., Kuze, A., Suto, H., and Grainger, R. G.: Retrieval and global assessment of terrestrial chlorophyll fluorescence from GOSAT space measurements, Remote Sensing of Environment, 121, 236-251, 10.1016/j.rse.2012.02.006, 2012.

Guanter, L., Zhang, Y., Jung, M., Joiner, J., Voigt, M., Berry, J. A., Frankenberg, C., Huete, A. R., Zarco-Tejada, P., Lee, J. E., Moran, M. S., Ponce-Campos, G., Beer, C., Camps-Valls, G., Buchmann, N., Gianelle, D., Klumpp, K., Cescatti, A., Baker, J. M., and Griffis, T. J.: Global and time-resolved monitoring of crop photosynthesis with chlorophyll fluorescence, Proceedings of the National Academy of Sciences of the United States of America, 111, E1327-1333, 10.1073/pnas.1320008111, 2014.

Hao, D., Asrar, G. R., Zeng, Y., Yang, X., Li, X., Xiao, J., Guan, K., Wen, J., Xiao, Q., Berry, J. A., and Chen, M.: Potential of hotspot solar-induced chlorophyll fluorescence for better tracking terrestrial photosynthesis, Glob Chang Biol, 10.1111/gcb.15554, 2021.

Heinsch, F. A., Maosheng, Z., Running, S. W., Kimball, J. S., Nemani, R. R., Davis, K. J., Bolstad, P. V., Cook, B. D., Desai, A. R., Ricciuto, D. M., Law, B. E., Oechel, W. C., Hyojung, K., Hongyan, L., Wofsy, S. C., Dunn, A. L., Munger, J. W., Baldocchi, D. D., Liukang, X., Hollinger, D. Y., Richardson, A. D., Stoy, P. C., Siqueira, M. B. S., Monson, R. K., Burns, S. P., and Flanagan, L. B.: Evaluation of remote sensing based terrestrial productivity from MODIS using regional tower eddy flux network observations, IEEE Transactions on Geoscience and Remote Sensing, 44, 1908-1925, 10.1109/tgrs.2005.853936, 2006.

Huete, A., Didan, K., Miura, T., Rodriguez, E. P., Gao, X., and Ferreira, L. G.: Overview of the radiometric and biophysical performanceof the MODIS vegetation indices, Remote Sensing of Environment, 83, 19, 2002.

Jiang, Z., Huete, A., Didan, K., and Miura, T.: Development of a two-band enhanced vegetation index without a blue band, Remote Sensing of Environment, 112, 3833-3845, 10.1016/j.rse.2008.06.006, 2008.

Joiner, J., Yoshida, Y., Vasilkov, A. P., Yoshida, Y., Corp, L. A., and Middleton, E. M.: First observations of global and seasonal terrestrial chlorophyll fluorescence from space, Biogeosciences, 8, 637-651, 10.5194/bg-8-637-2011, 2011.

Julitta, T.: Optical proximal sensing for vegetation monitoring, PhD Dissertation, Department of Earth and Environmental Sciences, University of Milano-Bicocca, 136 pp., 2015.

https://doi.org/10.5194/bg-2021-95
Preprint. Discussion started: 19 April 2021

Jung, M., Reichstein, M., Margolis, H. A., Cescatti, A., Richardson, A. D., Arain, M. A., Arneth, A., Bernhofer, C., Bonal, D., Chen, J., Gianelle, D., Gobron, N., Kiely, G., Kutsch, W., Lasslop, G., Law, B. E., Lindroth, A., Merbold, L., Montagnani, L., Moors, E. J., Papale, D., Sottocornola, M., Vaccari, F., and Williams, C.: Global patterns of land-atmosphere fluxes of carbon dioxide, latent heat, and sensible heat derived from eddy covariance, satellite, and meteorological observations, Journal of Geophysical Research, 116, 10.1029/2010jg001566, 2011.

Köhler, P., Guanter, L., Kobayashi, H., Walther, S., and Yang, W.: Assessing the potential of sun-induced fluorescence and the canopy scattering coefficient to track large-scale vegetation dynamics in Amazon forests, Remote Sensing of Environment, 769-785, 10.1016/j.rse.2017.09.025, 2017.

Lasslop, G., Reichstein, M., Detto, M., Richardson, A. D., and Baldocchi, D. D.: Comment on Vickers et al.: Self-correlation between assimilation and respiration resulting from flux partitioning of eddy-covariance CO2 fluxes, Agricultural and Forest Meteorology, 150, 312-314, 10.1016/j.agrformet.2009.11.003, 2010.

Lee, J. E., Frankenberg, C., van der Tol, C., Berry, J. A., Guanter, L., Boyce, C. K., Fisher, J. B., Morrow, E., Worden, J. R., Asefi, S., Badgley, G., and Saatchi, S.: Forest productivity and water stress in Amazonia: observations from GOSAT chlorophyll fluorescence, Proceedings. Biological sciences / The Royal Society, 280, 20130171, 10.1098/rspb.2013.0171, 2013.

Lewis, S. L., Lloyd, J., Sitch, S., Mitchard, E. T. A., and Laurance, W. F.: Changing Ecology of Tropical Forests: Evidence and Drivers, Annual Review of Ecology, Evolution, and Systematics, 40, 529-549, 10.1146/annurev.ecolsys.39.110707.173345, 2009.

Liangyun Liu, X. L., ZhihuiWang, and Bing Zhang: Measurement and Analysis of BidirectionalSIF Emissions in Wheat Canopies, IEEE TRANSACTIONS ON GEOSCIENCE AND REMOTE SENSING, 12, 2016.

Liu, J., Bowman, K. W., Schimel, D. S., Parazoo, N. C., Jiang, Z., Lee, M., Bloom, A. A., Wunch, D., Frankenberg, C., Sun, Y., O'Dell, C. W., Gurney, K. R., Menemenlis, D., Gierach, M., Crisp, D., and Eldering, A.: Contrasting carbon cycle responses of the tropical continents to the 2015-2016 El Nino, Science, 358, eaam5690, 10.1126/science.aam5690, 2017.

Liu, L., Yang, X., Gong, F., Su, Y., Huang, G., and Chen, X.: The Novel Microwave Temperature Vegetation Drought Index (MTVDI) Captures Canopy Seasonality across Amazonian Tropical Evergreen Forests, Remote Sensing, 13, 10.3390/rs13030339, 2021.

Liu, X., Liu, L., Zhang, S., and Zhou, X.: New Spectral Fitting Method for Full-Spectrum Solar-Induced Chlorophyll Fluorescence Retrieval Based on Principal Components Analysis, Remote Sensing, 7, 10626-10645, 10.3390/rs70810626, 2015.

Logan, B. A., Adams, W. W., and Demmig-Adams, B.: Viewpoint:Avoiding common pitfalls of chlorophyll fluorescence analysis under field conditions, Functional Plant Biology, 34, 853, 10.1071/fp07113, 2007.

Magney, T. S., Frankenberg, C., Fisher, J. B., Sun, Y., North, G. B., Davis, T. S., Kornfeld, A., and Siebke, K.: Connecting active to passive fluorescence with photosynthesis: a method for evaluating remote sensing measurements of Chl fluorescence, The New phytologist, 1594-1608, 10.1111/nph.14662, 2017.

Malenovsky, Z., Mishra, K. B., Zemek, F., Rascher, U., and Nedbal, L.: Scientific and technical challenges in remote sensing of plant canopy reflectance and fluorescence, Journal of experimental botany, 60, 2987-3004, 10.1093/jxb/erp156, 2009.

Meroni, M., Rossini, M., Guanter, L., Alonso, L., Rascher, U., Colombo, R., and Moreno, J.: Remote sensing of solar-induced chlorophyll fluorescence: Review of methods and applications, Remote Sensing of Environment, 113, 2037-2051, 10.1016/j.rse.2009.05.003, 2009.

Merrick, Pau, Jorge, Bennartz, and Silva: Spatiotemporal Patterns and Phenology of Tropical Vegetation Solar-Induced Chlorophyll Fluorescence across Brazilian Biomes Using Satellite Observations, Remote Sensing, 11, 10.3390/rs11151746, 2019.

Merrick, T., Jorge, M. L. S. P., Silva, T. S. F., Pau, S., Rausch, J., Broadbent, E. N., and Bennartz, R.: Characterization of chlorophyll fluorescence, absorbed photosynthetically active radiation, and reflectance-based vegetation index spectroradiometer measurements, International Journal of Remote Sensing, 41, 6755-6782, 10.1080/01431161.2020.1750731, 2020.

Mitchard, E. T. A.: The tropical forest carbon cycle and climate change, Nature, 559, 527-534, 10.1038/s41586-018-0300-2, 2018.

Morton, D. C., Rubio, J., Cook, B. D., Gastellu-Etchegorry, J. P., Longo, M., Choi, H., Hunter, M. O., and Keller, M.: Amazon forest structure generates diurnal and seasonal variability in light utilization, Biogeosciences Discussions, 12, 19043-19072, 10.5194/bgd-12-19043-2015, 2015.

Morton, D. C., Nagol, J., Carabajal, C. C., Rosette, J., Palace, M., Cook, B. D., Vermote, E. F., Harding, D. J., and North, P. R.: Amazon forests maintain consistent canopy structure and greenness during the dry season, Nature, 506, 221-224, 10.1038/nature13006, 2014.

https://doi.org/10.5194/bg-2021-95
Preprint. Discussion started: 19 April 2021

Moya, I., Camenen, L., Evain, S., Goulas, Y., Cerovic, Z. G., Latouche, G., Flexas, J., and Ounis, A.: A new instrument for passive remote sensing1. Measurements of sunlight-induced chlorophyll fluorescence, Remote Sensing of Environment, 91, 186-197, 10.1016/j.rse.2004.02.012, 2004.

Plascyk, J. A.: The MK II Fraunhofer Line Discriminator (FLD -II) for Airborne and Orbital Remote Sensing of Solar-Stimulated Luminescense, Optical Engineering, 14, 8, 1975.

Porcar-Castell, A., Tyystjarvi, E., Atherton, J., van der Tol, C., Flexas, J., Pfundel, E. E., Moreno, J., Frankenberg, C., and Berry, J. A.: Linking chlorophyll a fluorescence to photosynthesis for remote sensing applications: mechanisms and challenges, Journal of experimental botany, 65, 4065-4095, 10.1093/jxb/eru191, 2014.

R Development Core Team: R: A language and environment for statistical computing, R Foundation for Statistical Computing [code], 2010.

Rocha, A. V., Appel, R., Bret-Harte, M. S., Euskirchen, E. S., Salmon, V., and Shaver, G.: Solar position confounds the relationship between ecosystem function and vegetation indices derived from solar and photosynthetically active radiation fluxes, Agricultural and Forest Meteorology, 298-299, 10.1016/j.agrformet.2020.108291, 2021.

Rong Li, F. Z.: Accuracy assessment on reconstruction algorithms of solar-induced Fluorescence Spectrum, Geoscience and Remote Sensing Symposium (IGARSS) IEEE International, 1727-1730,

Rossini, M., Alonso, L., Cogliati, S., Damm, A., Guanter, L., Julitta, T., Meroni, M., Moreno, J., Panigada, C., Pinto, F., Rascher, U., Schickling, A., Schüttemeyer, D., Zemek, F., and Colombo, R.: Measuring sun-induced chlorophyll fluorescence: An evaluation and synthesis of existing field data, 5th International workshop on remote sensing of vegetation fluorescence, Paris, France, 1-5,

Rouse Jr, J. W., Haas, R. H., Schell, J. A., and Deering, D. W.: Paper A 20, hird Earth Resources Technology Satellite-1 Symposium: The Proceedings of a Symposium Goddard Space Flight Center at Washington, DC 309,

Running, S. W., Nemani, R. R., Heinsch, F. A., Zhao, M., Reeves, M., and Hashimoto, H.: A Continuous Satellite-Derived Measure of Global Terrestrial Primary Production, BioScience, 54, 547-551, 2004.

Ryu, Y., Jiang, C., Kobayashi, H., and Detto, M.: MODIS-derived global land products of shortwave radiation and diffuse and total photosynthetically active radiation at 5 km resolution from 2000, Remote Sensing of Environment, 204, 812-825, 10.1016/j.rse.2017.09.021, 2018.

Saatchi, S. S., Harris, N. L., Brown, S., Lefsky, M., Mitchard, E. T., Salas, W., Zutta, B. R., Buermann, W., Lewis, S. L., Hagen, S., Petrova, S., White, L., Silman, M., and Morel, A.: Benchmark map of forest carbon stocks in tropical regions across three continents, Proceedings of the National Academy of Sciences of the United States of America, 108, 9899-9904, 10.1073/pnas.1019576108, 2011.

Samanta, A., Ganguly, S., and Myneni, R.: MODIS Enhanced Vegetation Index data do not show greening of Amazon forests during the 2005 drought, New Phytologist, 189, 4, 2010.

Schickling, A., Matveeva, M., Damm, A., Schween, J., Wahner, A., Graf, A., Crewell, S., and Rascher, U.: Combining Sun-Induced Chlorophyll Fluorescence and Photochemical Reflectance Index Improves Diurnal Modeling of Gross Primary Productivity, Remote Sensing, 8, 574, 10.3390/rs8070574, 2016.

Sims, D., Rahman, A., Cordova, V., Elmasri, B., Baldocchi, D., Bolstad, P., Flanagan, L., Goldstein, A., Hollinger, D., and Misson, L.: A new model of gross primary productivity for North American ecosystems based solely on the enhanced vegetation index and land surface temperature from MODIS, Remote Sensing of Environment, 112, 1633-1646, 10.1016/j.rse.2007.08.004, 2008.

Springer, K., Wang, R., and Gamon, J. A.: Parallel Seasonal Patterns of Photosynthesis, Fluorescence, and Reflectance Indices in Boreal Trees, Remote Sensing, 9, 1-18, 10.3390/rs9070691, 2017.

Sun, Y., Frankenberg, C., Wood, J. D., Schimel, D. S., Jung, M., Guanter, L., Drewry, D. T., Verma, M., Porcar-Castell, A., Griffis, T. J., Gu, L., Magney, T. S., Kohler, P., Evans, B., and Yuen, K.: OCO-2 advances photosynthesis observation from space via solar-induced chlorophyll fluorescence, Science, 358, eaam5747, 10.1126/science.aam5747, 2017.

Torrence, C. and Compo, G. P.: A Practical Guide to Wavelet Analysis, Bulletin of the American Meteorological Society, 79, 61-79, 1998.

Turner, D. P., Ritts, W. D., Cohen, W. B., Gower, S. T., Zhao, M., Running, S. W., Wofsy, S. C., Urbanski, S., Dunn, A. L., and Munger, J. W.: Scaling Gross Primary Production (GPP) over boreal and deciduous forest landscapes in support of MODIS GPP product validation, Remote Sensing of Environment, 88, 256-270, 10.1016/j.rse.2003.06.005, 2003.

Van Wittenberghe, S., Alonso, L., Verrelst, J., Moreno, J., and Samson, R.: Bidirectional sun-induced chlorophyll fluorescence emission is influenced by leaf structure and light scattering properties — A bottom-up approach, Remote Sensing of Environment, 158, 169-179, 10.1016/j.rse.2014.11.012, 2015.

https://doi.org/10.5194/bg-2021-95
Preprint. Discussion started: 19 April 2021

Van Wittenberghe, S., Alonso, L., Verrelst, J., Hermans, I., Delegido, J., Veroustraete, F., Valcke, R., Moreno, J., and Samson, R.: Upward and downward solar-induced chlorophyll fluorescence yield indices of four tree species as indicators of traffic pollution in Valencia, Environmental pollution, 173, 29-37, 10.1016/j.envpol.2012.10.003, 2013.

Wang, C., Beringer, J., Hutley, L. B., Cleverly, J., Li, J., Liu, Q., and Sun, Y.: Phenology Dynamics of Dryland Ecosystems Along the North Australian Tropical Transect Revealed by Satellite Solar-Induced Chlorophyll Fluorescence, Geophysical Research Letters, 46, 5294-5302, 10.1029/2019gl082716, 2019.

Wang, S., Zhang, Y., Ju, W., Qiu, B., and Zhang, Z.: Tracking the seasonal and inter-annual variations of global gross primary production during last four decades using satellite near-infrared reflectance data, The Science of the total environment, 755, 142569, 10.1016/j.scitotenv.2020.142569, 2020.

Wickham, H.: ggplot2: Elegant Graphics for Data Analysis, Springer-Verlag [code], 2016.

Wickham, H.: tidyverse: Easily Install and Load the 'Tidyverse' (R package version 1.2.1) [code], 2017.

Wickham, H., François, R., Henry, L., and Müller, K.: dplyr: A Grammar of Data Manipulation (R package version 0.7.8) [code], 2018.

Wu, G., Guan, K., Jiang, C., Peng, B., Kimm, H., Chen, M., Yang, X., Wang, S., Suyker, A. E., Bernacchi, C. J., Moore, C. E., Zeng, Y., Berry, J. A., and Cendrero-Mateo, M. P.: Radiance-based NIRv as a proxy for GPP of corn and soybean, Environmental Research Letters, 15, 10.1088/1748-9326/ab65cc, 2020.

Xu, L., Saatchi, S. S., Yang, Y., Myneni, R. B., Frankenberg, C., Chowdhury, D., and Bi, J.: Satellite observation of tropical forest seasonality: spatial patterns of carbon exchange in Amazonia, Environmental Research Letters, 10, 084005, 10.1088/1748-9326/10/8/084005, 2015.

Yang, H., Yang, X., Zhang, Y., Heskel, M. A., Lu, X., Munger, J. W., Sun, S., and Tang, J.: Chlorophyll fluorescence tracks seasonal variations of photosynthesis from leaf to canopy in a temperate forest, Glob Chang Biol, 23, 2874-2886, 10.1111/gcb.13590, 2017.

Yang, J., Tian, H., Pan, S., Chen, G., Zhang, B., and Dangal, S.: Amazon droughts and forest responses: Largely reduced forest photosynthesis but slightly increased canopy greenness during the extreme drought of 2015/2016, Glob Chang Biol, 1919-1934, 10.1111/gcb.14056, 2018a.

Yang, K., Ryu, Y., Dechant, B., Berry, J. A., Hwang, Y., Jiang, C., Kang, M., Kim, J., Kimm, H., Kornfeld, A., and Yang, X.: Sun-induced chlorophyll fluorescence is more strongly related to absorbed light than to photosynthesis at half-hourly resolution in a rice paddy, Remote Sensing of Environment, 216, 658-673, 10.1016/j.rse.2018.07.008, 2018b.

Yang, P., van der Tol, C., Campbell, P. K. E., and Middleton, E. M.: Fluorescence Correction Vegetation Index (FCVI): A physically based reflectance index to separate physiological and non-physiological information in far-red sun-induced chlorophyll fluorescence, Remote Sensing of Environment, 240, 10.1016/j.rse.2020.111676, 2020.

Zarco-Tejada, P. J., González-Dugo, V., and Berni, J. A. J.: Fluorescence, temperature and narrow-band indices acquired from a UAV platform for water stress detection using a micro-hyperspectral imager and a thermal camera, Remote Sensing of Environment, 117, 322-337, 10.1016/j.rse.2011.10.007, 2012.

Zarco-Tejada, P. J., Morales, A., Testi, L., and Villalobos, F. J.: Spatio-temporal patterns of chlorophyll fluorescence and physiological and structural indices acquired from hyperspectral imagery as compared with carbon fluxes measured with eddy covariance, Remote Sensing of Environment, 133, 102-115, 10.1016/j.rse.2013.02.003, 2013.

Zarco-Tejada, P. J., Miller, J. R., Mohammed, G. H., Noland, T. L., and Sampson, P. H.: Estimation of chlorophyll fluorescence under natural illumination from hyperspectral data, International Journal of Applied Earth Observation and Geoinformation, 3, 7, 2001.

Zeng, Y., Badgley, G., Dechant, B., Ryu, Y., Chen, M., and Berry, J. A.: A practical approach for estimating the escape ratio of near-infrared solar-induced chlorophyll fluorescence, Remote Sensing of Environment, 232, 10.1016/j.rse.2019.05.028, 2019.

Zhang, Z., Zhang, Y., Zhang, Q., Chen, J. M., Porcar-Castell, A., Guanter, L., Wu, Y., Zhang, X., Wang, H., Ding, D., and Li, Z.: Assessing bi-directional effects on the diurnal cycle of measured solar-induced chlorophyll fluorescence in crop canopies, Agricultural and Forest Meteorology, 295, 10.1016/j.agrformet.2020.108147, 2020.

Zhao, M., Running, S., Heinsch, F. A., and Nemani, R.: MODIS-Derived Terrestrial Primary Production, 11, 635-660, 10.1007/978-1-4419-6749-7_28, 2010.